CHEMISTRY OF MATERIALS
Cite This: Chem. Mater. 2018, 30, 5968−5977
Article
pubs.acs.org/cm

Interaction of a Poly(phenylene vinylene) with an Organometallic Lewis Acid Additive: Fundamentals and Application in Polymer Solar Cells

Jiliang Wang,[†] Randi S. Price,[†] Gyu Leem,[‡] Junlin Jiang,[†] Khalil A. Abboud,[†] and Kirk S. Schanze*[,‡]

[†]Department of Chemistry, University of Florida, Gainesville, Florida 32611, United States
[‡]Department of Chemistry, University of Texas at San Antonio, San Antonio, Texas 78249, United States

Supporting Information

ABSTRACT: The trimeric perfluoro-*o*-phenylene mercury compound Hg3 and poly(2-methoxy,5-(2′-ethylhexyloxy)-1,4-phenylenevinylene (MEH-PPV) interact strongly in solution and the solid state. The interaction is attributed to electron donor−acceptor complex formation, where MEH-PPV is the donor, and the Lewis acid Hg3 is the acceptor. The study reported herein explores the effects of the donor−acceptor complex formation on the properties of MEH-PPV in solution and in the solid state. Addition of Hg3 to MEH-PPV solution or films leads to a distinct color change, and the change in the visible absorption spectrum and fluorescence of MEH-PPV is consistent with the formation of polymer aggregates. In the solid state, Hg3 induced aggregation is suggested to lead to formation of crystalline domains of the conjugated polymer. Transmission electron microscopy and grazing incidence X-ray scattering results support the hypothesis that the complex formation with Hg3 induces aggregation of the polymer. Transient absorption spectroscopy of the MEH-PPV:Hg3 aggregates in *o*-dichlorobenzene solution reveals ultrafast exciton dissociation to generate the MEH-PPV positive polaron, formed via photoinduced electron transfer to the Hg3 as an electron acceptor. The X-ray crystal structure of a 1:1 complex between oligo(phenylene vinylene) and Hg3 gives insight into the structural interactions that likely account for the Hg3 induced polymer aggregation. Addition of small amounts of Hg3 to MEH-PPV:$PC_{61}BM$ bulk heterojunction solar cells results in a 33% increase in the power conversion efficiency, due to an increase in both the short-circuit photocurrent and open-circuit voltage. These factors are attributed to enhanced exciton dissociation coupled with improved carrier transport, resulting from the MEH-PPV:Hg3 donor−acceptor interaction.

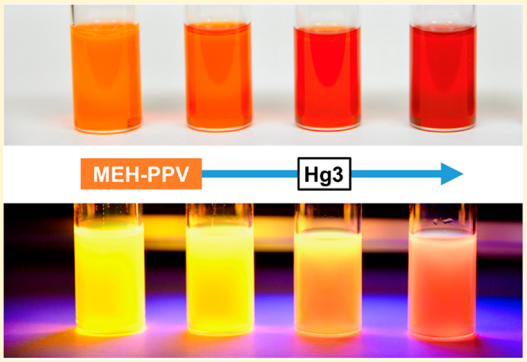

INTRODUCTION

Polymer solar cells (PSCs) have been investigated extensively as a next generation of clean energy source due to various advantages such as flexibility, lightweight, and low cost.[1−4] In the past few years, the development of new materials, processing methods, and device architectures has boosted the power conversion efficiency (PCE) of PSCs to greater than 10%.[5] For a bulk heterojunction (BHJ) device, the morphology of the donor and acceptor blend in the active layer is one of the key factors that influence device performance.[6] Some well-known strategies to optimize the BHJ active layer morphology are side-chain modification, thermal annealing, and solvent additives.[7] However, the approach of blending a small amount of solid additive into the active layer remains less studied. Chang et al. demonstrated a 50% increase of PCE by blending platinum nanoparticles (Pt NPs) into an active layer that consisted of poly(3-hexylthiophene-2,5-diyl) (P3HT) and [6,6]-phenyl-C61-butyric acid methyl ester ($PC_{61}BM$).[8] The resulting efficiency improvement was attributed to the increased carrier mobility in the active layer. Yu et al. reported that copper phthalocyanine (CuPc) can also be used as an active layer in the same P3HT:$PC_{61}BM$ system, and they attributed the 19% PCE increase to broadened absorption range and improved charge separation and transport properties.[9]

Previously, Gabbai and co-workers discovered unique supramolecular interactions between aromatic hydrocarbons (e.g., benzene, biphenyl, fluorene, naphthalene, diphenylacetylene) and the trimeric perfluoro-*ortho*-phenylene mercury compound Hg3 (Chart 1).[10−14] Their work shows that aromatic hydrocarbons (AHCs) and Hg3 form compact alternating stacks in a sandwich-like configuration in solid-state cocrystals. Density functional theory (DFT) calculations suggest that these interactions are likely electrostatic in nature, as the center of the trinuclear macrocycle of Hg3 has a positive electrostatic potential while the perimeter is negative.[10,15] In essence, Hg3 serves as a Lewis acid, and interacts with the AHCs in a donor−acceptor (DA) motif. In addition to the DA

Received: May 21, 2018
Revised: August 3, 2018
Published: August 5, 2018

DOI: 10.1021/acs.chemmater.8b02152
Chem. Mater. 2018, 30, 5968−5977

Chart 1. Structures of Hg3, MEH-PPV, and BP-PV

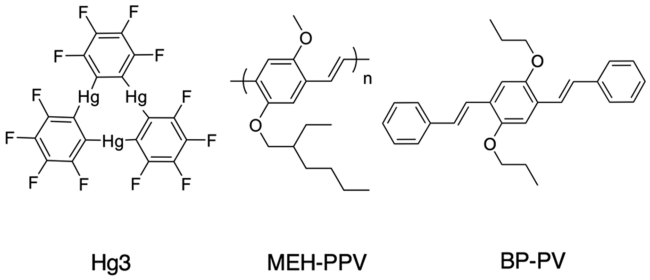

interaction, it was shown in the previous studies that the cocrystals of Hg3 and AHCs exhibit strong phosphorescence from the AHC. This effect presumably arises due to enhanced singlet−triplet intersystem crossing in the AHC promoted by the spin−orbit coupling from the heavy metal Hg3 complex.

Poly(2-methoxy,5-(2′-ethylhexyloxy)-1,4-phenylenevinylene (MEH-PPV, Chart 1) is one of the first conjugated polymers that demonstrated an efficient photovoltaic effect in BHJ solar cells. Consequently, it has served as a model conjugated polymer in many studies for the understanding and optimization of BHJ materials and cells.[16−18] In addition, there have been numerous studies that explored the effects of additives and solvents on the aggregation of MEH-PPV in solution and in the solid state. This work has correlated the structure and aggregation of MEH-PPV on its optical properties, as well as on the performance of organic solar cells based on blends of the polymer with $PC_{61}BM$.[19−21]

In the current study, we explored the interactions between Hg3 in solution and in films by using steady-state and time-resolved optical spectroscopy, X-ray scattering and in organic electronic devices, including ternary solar cells consisting of MEH-PPV/$PC_{61}BM$ and Hg3. This study reveals that there is a strong interaction between the organometallic Lewis acid and the aromatic polymer, both in solution and in the solid state. This interaction gives rise to ordering of the MEH-PPV chains, which is established by X-ray scattering. A cocrystal structure of an oligo(phenylene vinylene) oligomer (OPV) and Hg3 provides insight into the interactions between the Lewis acid and the conjugated chain. In addition, transient absorption spectroscopy reveals that Hg3 acts as an electron acceptor, giving rise to enhanced exciton splitting into electron/hole pairs. We also examined Hg3 as an active layer additive for BHJ PSCs containing MEH-PPV and $PC_{61}BM$ as donor and acceptor materials, which resulted in a 33% increase of PCE. This improvement is likely due to the enhanced exciton splitting that arises from the Hg3 acting as an electron acceptor.

EXPERIMENTAL SECTION

Unless specified, all compounds and solvents were purchased from commercial sources and used without further purification. MEH-PPV and $PC_{61}BM$ were purchased from American Dye Source Inc. Poly(3,4-ethylenedioxythiophene)-poly(styrenesulfonate) (PEDOT-PSS) (Baytron P VP Al 4083) solution was purchased from Heraeus Deutschland GmbH & Co. KG. Hydroquinone, tri(*n*-butyl) phosphine, 1-bromopropane, paraformaldehyde, glacial acetic acid, HBr (31%), benzaldehyde, potassium *tert*-butoxide, potassium hydroxide, toluene, diethyl ether, tetrahydrofuran, and all other chemicals were purchased from either Sigma-Aldrich or Fisher Chemicals.

^1H and ^{13}C nuclear magnetic resonance (NMR) spectra were measured on a Bruker Inova 500. Chemical shifts were referenced to the residual solvent peaks. ^1H NMR data were recorded with residual internal $CDCl_3$ (δ 7.26), and ^{13}C NMR data were recorded with reference $CDCl_3$ (δ 77.16). High resolution mass spectrometry was performed on a Bruker APEX II 4.7 T Fourier Transform Ion Cyclotron Resonance mass spectrometer.

UV−visible absorption measurements were carried out on a Shimadzu UV-1800 dual-beam spectrophotometer. Fluorescence emission measurements were carried out on a Photon Technology International QuantaMaster spectrophotometer. Grazing incidence wide-angle X-ray scattering (GIWAXS) measurements were carried out at the Stanford Synchrotron Radiation Lightsource SSRL on beamline 11-3 with a wavelength of 0.9742 Å. Samples were made by either spin-coating or drop-coating on silicon substrates. Transmission electron microscopy (TEM) imaging was carried out on a JEOL 2010F transmission electron microscope at 200 kV operating voltage. Sample films were made by spin-coating on PEDOT-PSS covered substrates. After PEDOT-PPS layers were dissolved in deionized water, films were caught by copper grids and dried overnight. Film thickness measurements were carried out on a Dektak 150 profilometer.

Femtosecond transient absorption measurements were carried out on an Ultrafast Systems Helios Fire transient absorption spectrometer. The output beam (800 nm) of a Coherent Astrella Ti:saphire pulsed laser (120 fs, 1 kHz) was split into pump and probe beams. The pump was passed through a Coherent OPerA Solo optical parametric amplifier to tune the excitation wavelength (290−2600 nm) prior to entering the spectrometer. Inside the spectrometer, the pump was passed through a mechanical chopper, depolarizer, and neutral density filter to tune the pump power to 0.1 mW (100 nJ/pulse). The probe beam entered the spectrometer and passed through a computer-controlled 8 ns delay stage and wavelength specific crystals to adjust the spectral region of the probe beam (sapphire for visible, 420−780 nm; and an Ultrafast Systems proprietary crystal for NIR, 820−1500 nm). Samples were continuously stirred in a cuvette with a 2 mm path length at the location of pump−probe overlap, where the laser spot size was about 435 μm. The signal from the probe beam was detected using a fiber-coupled alignment free spectrometer at either a visible (1024 pixel CMOS) or NIR (256 pixel InGaAs) detector with a time resolution of 250 fs. Chirp and time-zero corrected spectra and multiexponential kinetic fits were acquired and manipulated using SurfaceExplorer software (Ultrafast Systems). Energy dependent spectra were achieved in like fashion, and by adjusting the pump neutral density filter to vary the power from 0.05 to 0.4 mW, measured near the sample location with a power meter (ThorLabs PM100A). Nanosecond transient absorption spectroscopy was carried out on a system that has been previously described.[22]

Polymer solar cells were fabricated using prepatterned indium tin oxide (ITO)-covered glass as substrates (KINTEC Company). The ITO glass substrates were subsequently cleaned with aqueous sodium dodecyl sulfate, deionized water (18 MΩ, Milli-Q), acetone, and isopropyl alcohol for 15 min, respectively, in an ultrasonic bath. After sonication, the substrates were then exposed to oxygen plasma for 20 min (Harrick PDC-32G). Then a layer of PEDOT-PSS with 30 nm film thickness was spin-coated on the ITO substrates. The active layer mixed solutions then were deposited onto the PEDOT-PSS covered substrates in an Ar atmosphere glovebox (MBraun, H_2O and O_2 < 0.1 ppm). Electrodes were deposited by a thermal evaporator under vacuum in the glovebox (1×10^{-6} mbar). Solar cells were characterized under AM1.5 condition (100 mW/cm^2) and the current density and voltage $J-V$ characteristics were measured by a Keithley 2400 sourcemeter. Incident photon-to-electron conversion efficiency (IPCE) measurement was done with a 150 W Xe arc lamp coupled with an Oriel Cornerstone 130 monochromator. The incident radiation power was determined by a calibrated UDT Instrument 211 photodiode. Hole mobility of space charge limited current (SCLC) devices was calculated according to $J = \frac{9}{8}\varepsilon_r\varepsilon_0\mu_0 \exp(0.891\gamma\sqrt{E})\frac{V^2}{L^3}$, where ε_r = 4 was used.

X-ray intensity data were collected at 100 K on a Bruker DUO diffractometer using Mo Kα radiation (λ = 0.71073 Å) and an APEXII

DOI: 10.1021/acs.chemmater.8b02152
Chem. Mater. 2018, 30, 5968−5977

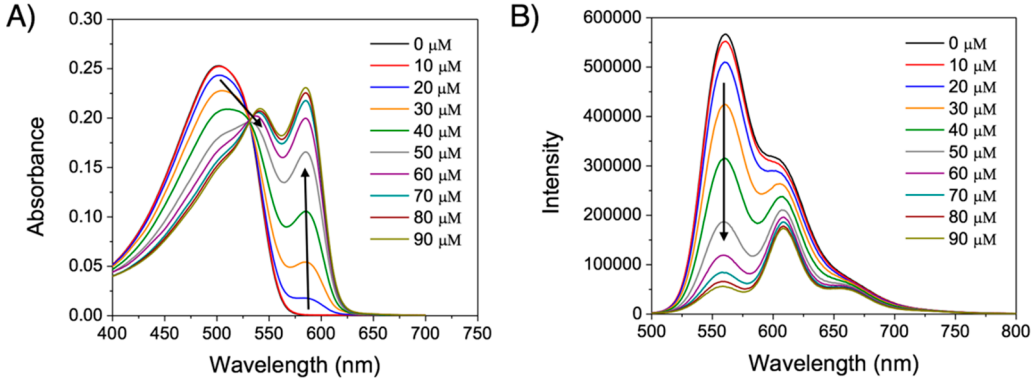

Figure 1. (A) UV−visible absorption spectra and (B) fluorescence emission spectra of MEH-PPV (15 μM) in chlorobenzene with an increasing concentration of Hg3 (0−90 μM). All experiments were performed at room temperature. 480 nm was used as the excitation wavelength for fluorescence emission measurements.

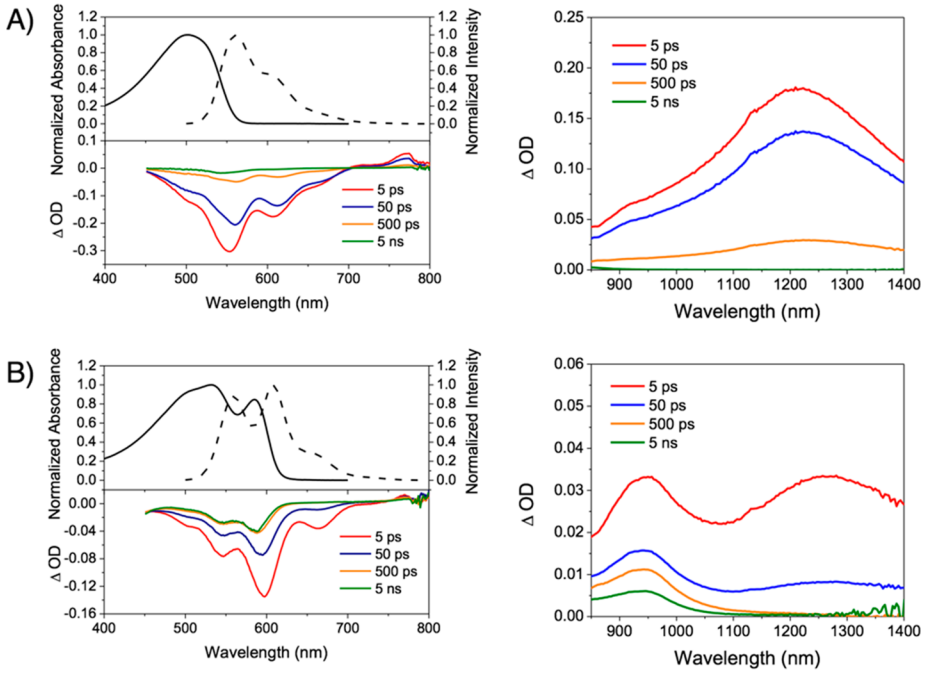

Figure 2. UV−visible absorption, fluorescence emission, and femtosecond transient absorption composite spectra of 600 μM MEH-PPV in chlorobenzene with (A) 0 μM and (B) 225 μM Hg3, respectively. All samples were excited using femtosecond pulses (λ = 420 nm, 100 nJ/pulse).

CCD area detector. Raw data frames were read by the program SAINT[1] and integrated using 3D profiling algorithms. The resulting data were reduced to produce *hkl* reflections and their intensities and estimated standard deviations. The data were corrected for Lorentz and polarization effects, and numerical absorption corrections were applied based on indexed and measured faces. The structure was solved and refined in SHELXTL2013, using full-matrix least-squares refinement. The non-H atoms were refined with anisotropic thermal parameters, and all of the H atoms were calculated in idealized positions and refined riding on their parent atoms. The asymmetric unit consists of an Hg3 complex, two half ligands, and a dichloromethane solvent molecule. The ligands are located on inversion symmetry centers. In the final cycle of refinement, 9940 reflections (of which 8987 are observed with $I > 2\sigma(I)$) were used to refine 595 parameters and the resulting R_1, wR_2, and S (goodness of fit) were 1.61%, 3.73%, and 1.094, respectively. The refinement was carried out by minimizing the wR_2 function using F^2 rather than F values. R_1 is calculated to provide a reference to the conventional R value, but its function is not minimized.

RESULTS AND DISCUSSION

Effect of Hg3 on the Photophysical Properties of MEH-PPV in Solution. Initially, we explored the interactions of Hg3 and MEH-PPV by mixing the materials in solution. The interactions were found to be solvent dependent, and the most pronounced effects were observed in aromatic hydrocarbons such as benzene and chlorobenzene. In these solvents, addition of Hg3 to the polymer leads to marked color changes in the solution (e.g., orange to wine-red; see TOC graphic). In order to quantify these effects, UV−visible absorption and fluorescence emission spectra of MEH-PPV in chlorobenzene with an increasing concentration of Hg3 were measured, and the results are shown in Figure 1A. The MEH-PPV solution features a strong absorption peak at $\lambda \sim 500$ nm, whereas the pure Hg3 solution has no absorption in the visible region. Interestingly, upon addition of Hg3 to a solution of MEH-PPV, the polymer's absorption band gradually red-shifts toward 550 nm and another peak arises at $\lambda \sim 590$ nm. These spectral changes suggest that Hg3 induces aggregation of MEH-PPV,

DOI: 10.1021/acs.chemmater.8b02152
Chem. Mater. 2018, 30, 5968−5977

Table 1. Transient Absorption Decay Lifetimes of the Singlet Excited State of MEH-PPV in Chlorobenzene with an Increasing Concentration of Hg3[b]

	τ/ps			$\langle\tau\rangle$/ps[a]		
λ (nm)	0 μM	150 μM	225 μM	0 μM	150 μM	225 μM
1250	4.4 (12.3%)	0.6 (53.4%)	0.2 (77.2%)	237.5	28.3	4.2
	114.2 (32.0%)	8.3 (26.8%)	3.4 (15.8%)			
	360.1 (55.7%)	133.3 (19.4%)	53.1 (6.7%)			
950		0.6 (54.1%)	0.3 (70.2%)		54.2	24.0
		12.7 (23.8%)	6.1 (18.7%)			
		328.1 (15.5%)	332.8 (6.8%)			

[a]Amplitude weighted median lifetime calculated as follows: $<\tau> = A_1\tau_1 + A_2\tau_2 + A_3\tau_3$. [b]The three samples have 0 μM, 150 μM, and 225 μM of Hg3.

because they are consistent with the spectral changes reported in a previous study where aggregation of MEH-PPV in solution was induced by the addition of a nonsolvent.[23]

The same phenomenon was also observed in spin-coated MEH-PPV thin films. Figure S1 shows how the UV−visible absorption of MEH-PPV thin films experienced similar spectral changes when an increasing amount of Hg3 was added. We conclude that the spectral changes of MEH-PPV in solution and films induced by Hg3 are the result of an electron donor−acceptor interaction, where the Hg3 acts as the acceptor, and the MEH-PPV as donor. The interaction leads to aggregation of the polymer chains.[24] In fact, in more concentrated MEH-PPV solution, Hg3 caused polymer chains to aggregate to the extent of precipitating out of the solution.

The optical properties of MEH-PPV are dependent on the conformation and aggregation state of polymer chains in solution and films.[25,26] Panzer et al. reported that MEH-PPV chains go from a random coil conformation to a crystallized aggregate conformation as the temperature of the solution was lowered.[27] The UV−visible absorption spectral changes they observed during this transformation are identical to ones MEH-PPV solution demonstrated when Hg3 was gradually added. This similarity suggests that Hg3 not only induces the aggregation of MEH-PPV but also helps the polymer chains to aggregate in a more ordered crystalline form.

As shown in Figure 1B, addition of Hg3 to a solution of MEH-PPV also induces considerable changes in the polymer's fluorescence spectrum. With increasing concentration of Hg3, the fluorescence intensity decreases (quenched), and at a certain concentration, the emission no longer changes. At this point, it is characterized by a new fluorescence band manifold with the 0-0 at ∼610 nm which is red-shifted by nearly 50 nm from the 0-0 band of the polymer. Similar changes in fluorescence of MEH-PPV have been previously observed, and attributed to aggregation of the polymer chains.[26,28]

In order to gain further insight regarding the basis for the effect of Hg3 on the MEH-PPV fluorescence, femtosecond transient absorption (TA) spectroscopy was used to probe the excited state dynamics of the polymer in chlorobenzene with varying concentration of Hg3. Selected spectra of pure MEH-PPV and MEH-PPV with 225 μM Hg3 are highlighted in Figure 2, and the full set of transient absorption spectra in both visible and near-IR regions are shown in Figure S2. In pure MEH-PPV solution (Figure 2A), both ground state bleaching and stimulated emission are observed in the visible region ranging from 450 to 700 nm, and singlet exciton absorption is observed in both visible and near-IR regions, with a weak band at ∼770 nm and a more intense one at ∼1250 nm. When Hg3 is added (Figure 2B), the visible and near-IR singlet exciton absorption is effectively decreased and decays much more rapidly (see below); in addition, a new transient absorption band at ∼950 nm appears and persists 5 ns after excitation.[29] The peak at $\lambda \sim 950$ nm corresponds to the absorption of the MEH-PPV radical cation (polaron) MEH-PPV$^{+\bullet}$,[30] signaling that MEH-PPV to Hg3 electron transfer (ET) occurs. This ET process helps to explain the decreased singlet excited state absorption and the quenching of fluorescence emission of MEH-PPV upon the addition of Hg3. Because of electron transfer, the singlet exciton of the polymer is depopulated, leading to the reduction of its intensity in transient absorption and quenching of its fluorescence emission.

Analysis of the decay kinetics of the singlet state TA of MEH-PPV shows that Hg3 electron transfer to Hg3 quenches the singlet exciton very rapidly. Specifically, the dynamics of the singlet exciton and polaron as a function of concentration of Hg3 was determined by fitting the TA dynamics at 1250 and 950 nm. The results are summarized in Table 1, and the decay plots are shown in Figure S3. At 1250 nm where only the singlet exciton absorbs, the decay lifetime components with the largest amplitude significantly shorten from the order of 100 ps to the order of 0.1 ps in the presence of Hg3 (see Table 1 and Figure S3A). This significantly increased decay rate shows that the singlet exciton is very rapidly quenched by addition of Hg3, presumably due to MEH-PPV to Hg3 electron transfer. The kinetics at 935 nm are more complicated, because there is overlapping absorption by the polaron and singlet exciton. At this wavelength, it is seen that the overall decay rate accelerates with increasing Hg3 concentration; this is presumably due to the contribution of the exciton decay to the transient absorption signal. A rise due to the formation of the polaron cannot be resolved; this is likely due to overlap of the exciton absorption (which is decaying on the same time scale). It is also noteworthy that the absorption assigned to the MEH-PPV polaron at 935 nm persists beyond 5 ns (Figure 2B), suggesting that a significant fraction of charge separated state has a relatively slow rate of charge recombination. The persistence of the polaron state at times > 5 ns is also confirmed by the persistent ground state bleach signal that peaks at 590 nm (Figure 2B).

In summary, the ultrafast transient absorption experiments done with MEH-PPV and Hg3 in solution reveal the following important features. First, the MEH-PPV singlet exciton is quenched very rapidly by Hg3 (c = 225 μM). Nearly 90% of the exciton population decays with a lifetime < 5 ps, as signaled by the fast decay of the near-IR absorption at 1250 nm and the stimulated emission in the visible. Compared to the decay lifetime of the exciton in pristine MEH-PPV (∼240 ps), this means that the major exciton decay pathway (>90%) in the

DOI: 10.1021/acs.chemmater.8b02152
Chem. Mater. 2018, 30, 5968−5977

Table 2. $J-V$ Characteristics of MEH-PPV/PCBM PSCs

Hg3 (wt %)	V_{oc}[a] (V)	J_{sc}[a] (mA/cm^2)	J_{sc}[b] (mA/cm^2)	FF[a] (%)	PCE[a] (%)
0[c]	0.8 ± 0.01	3.7 ± 0.1	4.0	48 ± 0.0	1.5 ± 0.03
2[c]	0.9 ± 0.01	4.5 ± 0.2	4.6	51 ± 0.6	2.0 ± 0.07
5	0.9 ± 0.01	4.3 ± 0.04	4.5	51 ± 1.0	1.9 ± 0.06
9	0.8 ± 0.02	2.5 ± 0.2	2.5	49 ± 2	1.0 ± 0.10

[a]Listed values are the averages of results from 32 pixels on 4 different devices. The errors reported are standard deviations in the measured values. [b]Listed values are the estimated by integration of the IPCE data shown in Figure 3. [c]Average active layer thicknesses are 72 and 71 nm for devices containing 0% and 2% of Hg3, respectively.

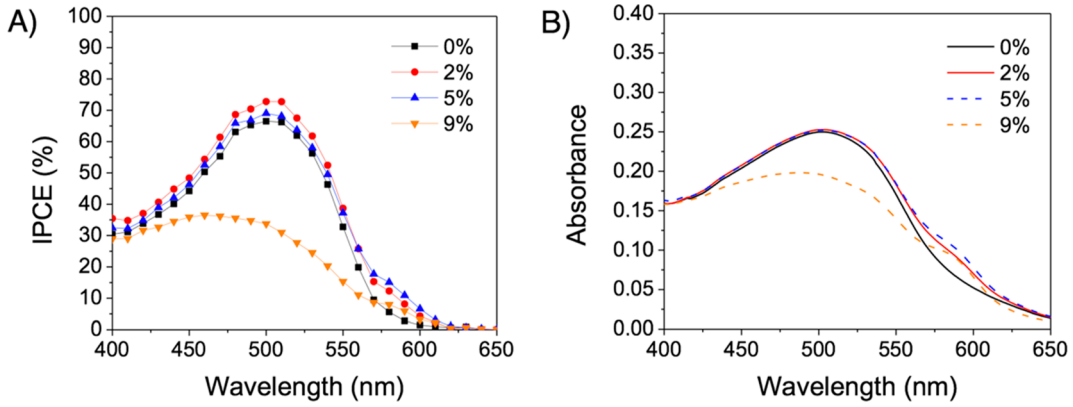

Figure 3. (A) IPCE spectra of four representative pixels and (B) UV−visible absorption spectra of corresponding active layers. Selected pixels are on devices containing 0%, 2%, 5%, and 9% of Hg3, respectively.

presence of Hg3 is due to electron transfer. Second, the electron transfer produces the MEH-PPV$^{+\bullet}$ polaron, as signaled by the 935 nm absorption band (which correlates with the literature precedent).[30] The polaron state decays on a time scale of 100 ps to 5 ns, presumably by charge recombination. However, it is evident that there is a fraction of the polaron that persists beyond 5 ns, as indicated by the persistent absorption at 935 nm and the ground state bleach in the visible region (590 nm). This indicates that some fraction of recombination takes place on a longer time scale.

As noted in the Introduction, previous work on complexes of Hg3 and aromatic hydrocarbons reveled room temperature phosphorescence from the solid crystals.[10−14] This work points to the possibility that Hg3 might give rise to enhanced singlet−triplet intersystem crossing (ISC) in the MEH-PPV/Hg3 complexes studied here. In order to probe for the triplet state in the MEH-PPV/Hg3 complexes, nanosecond transient absorption experiments were carried out (see Figure S4). These experiments reveal the presence of an MEH-PPV triplet absorption ($\lambda \sim 825$ nm) as well as the MEH-PPV polaron absorption ($\lambda \sim 950$ nm), which is also seen in the ultrafast experiments (Figure 2B). The triplet absorption intensity is not affected by the presence of Hg3, indicating that, in MEH-PPV/Hg3, there is not a significant change in the ISC efficiency. Moreover, careful experiments were performed at room temperature and low temperature in an attempt to detect phosphorescence in the near-IR from the MEH-PPV/Hg3 complexes, but these experiments were unsuccessful. We conclude that the predominant interaction between the polymer and Hg3 is of an electron donor−acceptor nature.

Effect of Hg3 on Performance of MEH-PPV:PC$_{61}$BM Solar Cells. Bulk heterojunction solar cells were fabricated and tested to examine the influence of Hg3 on device performance as an active layer additive. Devices were fabricated according to the structure ITO/PEDOT:PSS/active layer/lithium fluoride (LiF)/Al. The active layers contain MEH-PPV and PC$_{61}$BM (weight ratio 1:4) as the donor and acceptor materials,[6] and different amounts of Hg3 (0%, 2%, 5%, and 9%, weight percent relative to MEH-PPV). All devices were tested under AM1.5 illumination in air. Their current density and voltage ($J-V$) characteristics, including open-circuit voltage (V_{oc}), short-circuit current density (J_{sc}), fill factor (FF), and power conversion efficiency (PCE), are summarized in Table 2. Distribution histograms of PCE values of all tested devices are shown in Figure S4, and the $J-V$ curves of PSCs containing 0% and 2% of Hg3 are shown in Figure S5A.

The $J-V$ characteristics of devices without Hg3 (0%) are consistent with reported results obtained from similar conditions.[31] From 2% to 5% added Hg3, the $J-V$ characteristics, especially J_{sc} and PCE, increase with the concentration of Hg3. However, at 9% added Hg3, J_{sc} and PCE are substantially lower, indicating poorer cell performance. Therefore, an appropriate concentration of Hg3 improves the device performance, but when the concentration of Hg3 exceeds a threshold (apparently above 5%), additional Hg3 compromises the device performance. It should be noted that, in addition to the significant increase in J_{sc}, addition of Hg3 up to 5% induces a measurable increase in V_{oc} from 0.8 to 0.9 V. This effect may arise due to the influence of the Hg3 Lewis acid on lowering the HOMO of the polymer.

More insight into the effect of added Hg3 comes from studying the incident photon to current efficiency (IPCE) spectra for devices fabricated with varying amounts of Hg3 additive. The IPCE plots are compared to the absorption spectra of the active layer films in Figure 3. Here we note that the films used in this study were sufficiently thin such that the fraction of light absorbed across the entire visible region was less than 50%. In this situation, one expects the IPCE to mirror the absorption spectra of the active layers, and comparison of

DOI: 10.1021/acs.chemmater.8b02152
Chem. Mater. 2018, 30, 5968−5977

panels (A) and (B) in Figure 3 reveals this to be the case. However, close inspection of the IPCE spectra shows that, with addition of Hg3 to 2%, there is an overall increase in the photocurrent efficiency across the entire spectrum, combined with a noticeable small peak occurring at 580 nm which corresponds to the aggregate absorption band (cf. Figure 1A). This aggregate absorption can also be seen in the film absorption spectra for the same Hg3 compositions (Figure 3B). Upon further Hg3 increase to 5%, the IPCE shows a further increase at 580 nm, but now there is a small (and perhaps not differentiable within experimental error) decrease in the IPCE at the peak of the polymer's absorption.

Further increase of Hg3 to 9% induces a substantial decrease in the IPCE across the entire spectrum. The substantial change in IPCE at 9% Hg3 is also mirrored by a corresponding change in the absorption spectrum; this effect is partly associated with poorer film quality that arises with the higher Hg3 loading.

We posit that the influence of Hg3 on device performance arises for several reasons. First, at relatively low concentrations, the complex is able to induce crystalline order in the polymer phase, which enhances charge carrier mobility (*vide infra*). Second, as shown by the transient absorption results, Hg3 also is able to induce efficient exciton dissociation, as evidenced by the observation of the MEH-PPV polaron in mixtures of the polymer and the complex. However, the effect of ordering is limited to relatively low concentrations of the Hg3 additive. In fact, during device fabrication, it was observed that devices with 9% of added Hg3 showed visible clusters of MEH-PPV. This form of severe aggregation led to an active layer morphology detrimental to exciton diffusion and charge transport processes, which are two key processes to photocurrent generation.[4] Therefore, an appropriate amount of Hg3 (2%) acted as an efficient active layer additive in the bulk heterojunction PSCs and increased PCE by 33% compared to devices without Hg3.

Space charge limited current (SCLC) devices were fabricated and tested to understand the influence of Hg3 on hole mobility in the active layer of the PSCs. Hole-only SCLC devices were fabricated according to the structure ITO/PEDOT:PSS/active layer/Au. The active layers contain MEH-PPV and $PC_{61}BM$ (weight ratio 1:4) as the donor and acceptor materials, and different amounts of Hg3 (0% and 2%). The hole mobility and the thickness of the active layers of tested devices are summarized in Table 3, while the $J-V$ curves of SCLC devices containing 0% and 2% of Hg3 are shown in Figure S6B. With 2% of Hg3 in the active layer, the hole mobility increased from $1.8 \pm 0.14 \times 10^{-4}$ $cm^2/V{\cdot}s$ to $2.3 \pm 0.14 \times 10^{-4}$ $cm^2/V{\cdot}s$, while the thickness of the active layer remains essentially unchanged. We attribute the increase in hole mobility to a crystallized MEH-PPV phase induced by Hg3. The increased hole mobility in the active layer would likely improve the charge transport process in bulk heterojunction PSCs, and consequently could contribute to the enhancement of the device performance. However, it is important to note that a number of other factors could contribute to the Hg3-enhancement of the solar cell efficiency.

Table 3. Hole Mobility of SCLC Devices Containing 0% and 2% of Hg3

Hg3 (wt %)	thickness (nm)	μ_h[a] ($cm^2/V{\cdot}s$)
0	175 ± 1	$1.8 \pm 0.14 \times 10^{-4}$
2	173 ± 2	$2.3 \pm 0.14 \times 10^{-4}$

[a]Listed values are the averages of results from 8 pixels on 1 device. The errors reported are standard deviations in the measured values.

Effect of Hg3 on Morphology of MEH-PPV in Films. Transmission electron microscopy (TEM) was used to characterize the influence of Hg3 on the morphology of MEH-PPV in films. As shown in Figure 4A, an MEH-PPV film without Hg3 is amorphous with no distinctive features. By contrast, in the film that contained 20% of Hg3, MEH-PPV chains aggregated and formed a branch-like network structure within the film (Figure 4B). This aggregate polymer phase is likely to be more crystalline than the surrounding polymer phase. At the same time, Hg3 appears to self-aggregate, forming dot-shaped crystallites that can be seen in the left side image of Figure 4B. It should be noted that the films used for TEM characterization were pure MEH-PPV (without $PC_{61}BM$). Thus, 20% of Hg3 corresponds to a 1:4 weight ratio between Hg3 and MEH-PPV, which is the same as the weight ratio between Hg3 and MEH-PPV in a PSC device that contains 5% of Hg3. It is reasonable to conclude that an excessive amount of Hg3 not only induces significant aggregation of MEH-PPV chains but also introduces Hg3 crystallites as impurity, both of which result in significant disruption of the active layer morphology. Therefore, a decline of PSC device performance was observed, as the amount of Hg3 added in the active layer exceeded 2%.

Grazing incidence wide-angle X-ray scattering (GIWAXS) was used to examine the influence of Hg3 on the crystallinity of the polymer aggregate phase in MEH-PPV and MEH-PPV:$PC_{61}BM$ blend films. Diffractograms obtained from GIWAXS of MEH-PPV films containing increasing amounts of Hg3 are shown in Figure 5A. A distinctive peak at $q \sim 0.43$ $Å^{-1}$ arises as the concentration of Hg3 increases. This peak corresponds to a d-spacing of 14.6 Å, which is the lamellar distance of MEH-PPV in the crystalline region.[32] This finding reveals that Hg3 induces MEH-PPV to aggregate and form a more crystalline polymer phase in films, where the polymer chains are stacked in a more ordered pattern along the backbones. The other two minor peaks at $q \sim 0.68$ $Å^{-1}$ and $q \sim 0.97$ $Å^{-1}$ are due to Hg3 crystallites embedded in the films.

GIWAXS 2D images of MEH-PPV films, containing increasing amounts of Hg3, are shown in Figure 5B. The following changes in texture caused by the addition of Hg3 are observed. From 0% to 11% added Hg3, the outer ring shrinks and a dot on the q_z (vertical) axis appears and intensifies, due to the crystallization of MEH-PPV chains. From 11% to 20% added Hg3 and beyond, the dot on the q_z axis further intensifies, and a series of arcs appear on the q_{xy} (horizonal) axis, due to the further crystallization of MEH-PPV chains and the crystallization of Hg3 molecules.

On the basis of these observations, the following conclusions can be drawn. When the concentration of Hg3 was below 11%, Hg3 molecules mainly aggregated with MEH-PPV chains, which improved the crystallinity of the polymer phase. However, when the concentration of Hg3 exceeded 11% and approached 20%, Hg3 molecules started to also self-aggregate and form crystallites. In MEH-PPV films without $PC_{61}BM$, 11% of Hg3 corresponds to a 1:8 weight ratio between Hg3 and MEH-PPV, which is the same as the weight ratio between Hg3 and MEH-PPV in a MEH-PPV:$PC_{61}BM$ blend film that contains 2% of Hg3. Additionally, the changes in texture reveal that MEH-PPV adopted a random backbone orientation on

DOI: 10.1021/acs.chemmater.8b02152
Chem. Mater. 2018, 30, 5968−5977

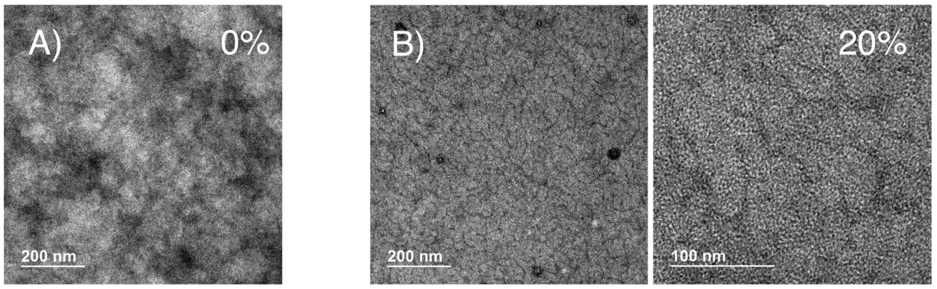

Figure 4. TEM images of MEH-PPV films containing (A) 0% and (B) 20% of Hg3 (wt %), respectively. Right side image in (B) is 2× magnification compared to left image.

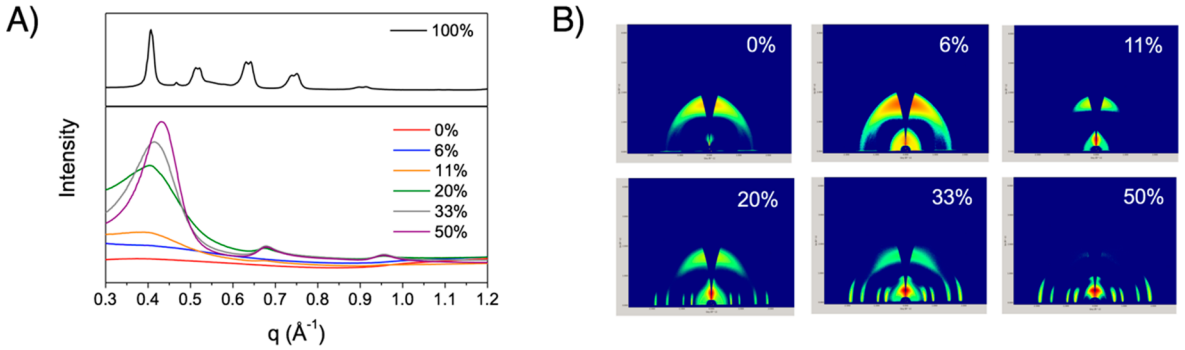

Figure 5. (A) GIWAXS diffractograms and (B) 2D images of drop-coated MEH-PPV films containing increasing amounts of Hg3 in wt %. 100% means pure Hg3 films made in the same way as the rest.

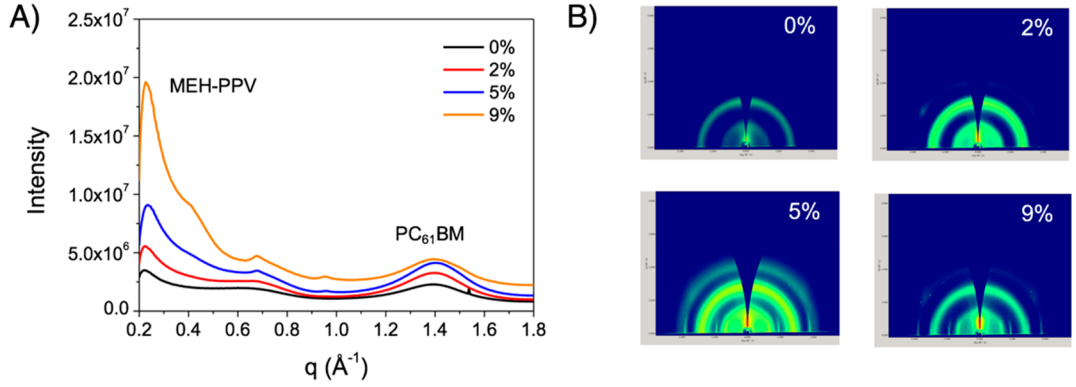

Figure 6. (A) GIWAXS diffractograms and (B) 2D images of spin-coated MEH-PPV:$PC_{61}BM$ blend films containing different amounts of Hg3 in wt %. All intensities are normalized to the thicknesses of films.

the substrate without Hg3, and the addition of Hg3 changed the backbone orientation to predominately edge-on.[33]

MEH-PPV:$PC_{61}BM$ blend films, containing increasing amounts of Hg3, were also examined by GIWAXS. The blend films were fabricated by spin-coating so that they represent the active layers of PSC devices discussed above. (Note that the studies of the pristine films described above were carried out with drop-cast films.) The diffractograms and 2D images of the spin-coated blend films are shown in Figure 6, and they show similar trends as observed in MEH-PPV films. When the concentration of Hg3 increases, two distinctive peaks arise that reflect MEH-PPV stacking and $PC_{61}BM$ stacking.[34] The MEH-PPV peak at $q \sim 0.22$ Å^{-1}corresponds to a *d*-spacing of 28.6 Å. This value is consistent with the bilayer lamellar distance in a solvent-induced transient structure of MEH-PPV, which would evolve into the regular MEH-PPV lamellar structure upon thermal annealing.[35] Because the MEH-PPV:$PC_{61}BM$ blend films were spin-coated, MEH-PPV chains were trapped in a thermodynamically unstable bilayer lamellar structure due to fast solvent evaporation. On the other hand, the pure MEH-PPV films were drop-coated; thus MEH-PPV chains adopted a thermodynamically stable regular lamellar structure directly. In fact, a closer inspection of Figure 6A reveals a shoulder at $q \sim 0.43$ Å^{-1}, which corresponds to a *d*-spacing of 14.6 Å. This value is identical to the lamellar distance observed in MEH-PPV films. Therefore, in the spin-coated blend films, MEH-PPV apparently adopts two stacking patterns, as shown in Scheme 1. The primary pattern is an unstable bilayer lamellar structure and the secondary pattern is a stable regular lamellar structure. And the MEH-PPV peak observed on the diffractograms is the result of the overlapping of two peaks relating to the two stacking patterns.

According to the texture changes on 2D images, the following conclusions can be drawn. When the concentration of Hg3 is below 2%, Hg3 molecules are mainly aggregated with MEH-PPV chains, which improved the crystallinity of the

DOI: 10.1021/acs.chemmater.8b02152
Chem. Mater. 2018, 30, 5968−5977

Scheme 1. An Illustration of the Two MEH-PPV Stacking Patterns: (A) Bilayer Lamellar Structure and (B) Regular Lamellar Structure

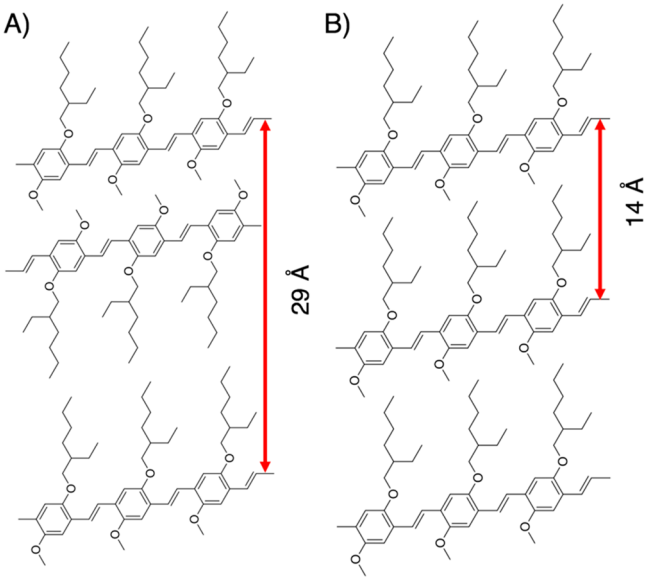

polymer phase. When the concentration of Hg3 exceeds 2%, Hg3 molecules self-aggregate, forming crystallites. Furthermore, MEH-PPV adopted a random backbone orientation on the substrate without Hg3, but the addition of Hg3 changed the backbone orientation to predominately edge-on. Since MEH-PPV:$PC_{61}BM$ blend films were fabricated in a manner that resembled the active layer of PSC devices, this finding reveals two possible interactions when Hg3 is added in the active layer of PSCs: Hg3 inducing the aggregation MEH-PPV and Hg3 self-aggregation. The former helps to improve the crystallinity of the active layer that facilitates the photocurrent generation, while the latter introduces impurity in the active layer that impedes the photocurrent generation. Therefore, it is crucial to ensure an appropriate weight ratio between Hg3 and MEH-PPV in the active layer so that Hg3 self-aggregation is suppressed and PCE is maximized. According to the results discussed, the optimal weight ratio between Hg3 and MEH-PPV is 1:8, which corresponds to 2% of Hg3 added in the active layer of MEH-PPV:$PC_{61}BM$ blend.

Crystal Structure of Model Compound and Hg3. To further understand the molecular interaction between MEH-PPV and Hg3, a small molecule 2,5-bis(propoxy)-1,4-bis-(phenylenevinylene)benzene (BP-PV, Chart 1) featuring the repeating unit of MEH-PPV was used as a model compound. The synthesis and characterization information on BP-PV can be found in the Supporting Information (Scheme S1 and Figures S6–S11). The 1:1 crystalline complex [BP-PV·Hg3] was grown by slow evaporation of a mixed solution of BP-PV and Hg3 (molar ratio 1:1). Single crystal X-ray crystallography analysis revealed the structure of [BP-PV·Hg3], as shown in Figure 7. Due to electrostatic interaction between the donor BP-PV and the electrophilic Hg3, the two molecules stack in a sandwich-like alternating configuration, which is consistent with previous studies on Hg3 with other aromatic small

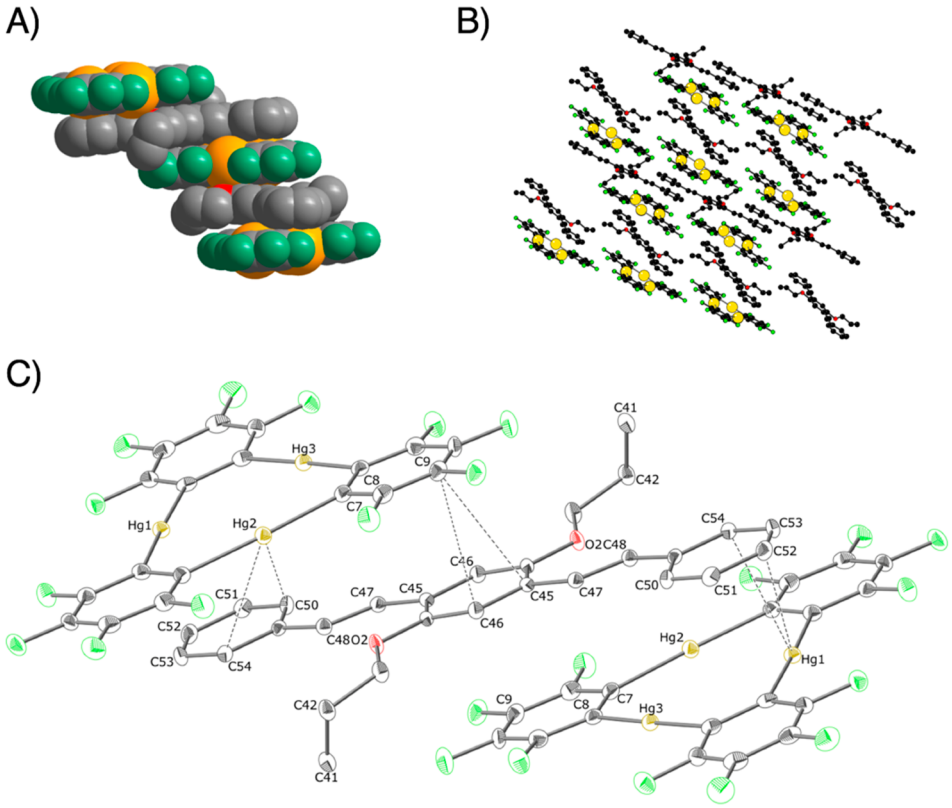

Figure 7. Illustrations of the crystal structure of [BP-PV·Hg3]. C atoms are colored black, F atoms are colored green, Hg atoms are colored yellow, and H atoms are omitted for clarity. (A) Space-filling model. (B) Ball-and-stick model showing an expanded scale. (C) Thermal ellipsoids model and representative intermolecular distances in Å: Hg(2)–C(50) 5.34, Hg(2)–C(54) 4.50, Hg(1)–C(52) 3.83, Hg(1)–C(54) 3.28, C(9)–C(45) 3.46, C(9)–C(46) 3.35.

DOI: 10.1021/acs.chemmater.8b02152
Chem. Mater. 2018, 30, 5968–5977

molecules (e.g., benzene, biphenyl, fluorine, naphthalene, diphenylacetylene).[14] Since BP-PV resembles the repeating unit of MEH-PPV, it is reasonable to conclude that the repeating units of MEH-PPV interact with Hg3 in a similar fashion, leading to the crystallization of MEH-PPV phase upon the addition of Hg3.

Given that only a small amount of Hg3 is needed to crystallize MEH-PPV, the complex molecules act like anchors that fix polymer chains in place by electrostatic forces and reduce their degree of freedom in movement. The repeating units of MEH-PPV and Hg3 trinuclear macrocycles stack upon one another in a sandwich-like alternating fashion. Because of this anchoring effect, MEH-PPV chains are able to aggregate in an ordered pattern and form a lamellar structure through interchain $\pi-\pi$ interaction. The increased degree of crystallinity in the polymer phase reduces disorder effects, e.g., energy traps and scattering sites, and ensures stronger $\pi-\pi$ electronic coupling between polymer chains, especially along the π stacking direction.[36−38] Both reduction of disorder effects and enhancement of $\pi-\pi$ electronic coupling are desired for more efficient exciton diffusion and charge transport,[39] which are the key steps of photocurrent generation.[4] Additionally, the charge transfer process observed between the excited MEH-PPV and Hg3 revealed a strong $\pi-\pi$ electronic coupling between the two species, confirming a viable pathway for charge transport even along the previously described sandwich-like stacks. Consequently, the addition of Hg3 to MEH-PPV:$PC_{61}BM$ blend results in an increased hole mobility and improved performance in PSC devices.

Since the electrophilic Hg3 is capable of interacting with various aromatic small molecules and form sandwich-like stacks,[14] we envision that Hg3 would also interact with various other conjugated polymers in a similar way as it does with MEH-PPV, and this electrostatic interaction would help to increase the degree of crystallinity of these polymers in the solid state. Therefore, as an active layer additive, the application of Hg3 is not limited to systems based on MEH-PPV, but also possible in systems using other conjugated polymers as donors or acceptors.[3] Beside PSC, conjugated polymers are used in many other electronic devices, e.g., organic field effect transistor (OFET), where the crystallinity of the polymer phase is crucial to device performance.[40] Therefore, as a crystallization agent, the application of Hg3 should not be limited to PSC, but also possible in other polymer-based electronic devices.

CONCLUSION

A trimeric perfluoro-*o*-phenylene mercury compound Hg3 was used as a novel active layer additive material for BHJ PSCs based on the MEH-PPV:$PC_{61}BM$ blend system. In solution, due to electrostatic forces, Hg3 induced MEH-PPV chains to aggregate and a charge transfer process between excited MEH-PPV and Hg3 was observed. In films, Hg3 molecules acted as anchors that forced MEH-PPV chains to form a more ordered lamellar structure, which increased the degree of crystallinity of the polymer phase. Due to reduced disorder effects and enhanced $\pi-\pi$ electronic coupling, exciton diffusion and charge transport efficiencies during photocurrent generation are both improved. As a result, the addition of 2% of Hg3 in the active layer increased PCE by 33%, confirming Hg3 as an effective active layer additive for PSCs.

ASSOCIATED CONTENT

Supporting Information

The Supporting Information is available free of charge on the ACS Publications website at DOI: 10.1021/acs.chemmater.8b02152.

Absorption spectra of MEH-PPV:Hg3 blend films, full data set for ultrafast transient absorption studies of MEH-PPV with added Hg3 in chlorobenzene, statistical data for MEH-PPV:PCBM:Hg3 solar cells, example $J-V$ curves for representative solar cell and SCLC devices, full synthesis experimental section, including characterization data for oligomer BP-PV (PDF)

Crystallographic data for BP-PV·Hg3 complex(CIF)

AUTHOR INFORMATION

ORCID

Gyu Leem: 0000-0003-0169-1096

Kirk S. Schanze: 0000-0003-3342-4080

Notes

The authors declare no competing financial interest.

ACKNOWLEDGMENTS

We acknowledge the National Science Foundation (Grant No. CHE-1737714) for support of this work. Hg3 was synthesized by Dr. Kye-Young Kim according to reported procedures.[41] X-ray scattering studies were carried out at Beamline 11-3 of the Stanford Synchrotron Radiation Lightsource, SLAC National Accelerator Laboratory, which is supported by the U.S. Department of Energy, Office of Science, Office of Basic Energy Sciences, under Contract No. DE-AC02-76SF00515.

REFERENCES

(1) Hoppe, H.; Sariciftci, N. S. Organic Solar Cells: An Overview. *J. Mater. Res.* **2004**, *19*, 1924−1945.

(2) Heeger, A. J. Semiconducting Polymers: The Third Generation. *Chem. Soc. Rev.* **2010**, *39*, 2354−2371.

(3) Lu, L.; Zheng, T.; Wu, Q.; Schneider, A. M.; Zhao, D.; Yu, L. Recent Advances in Bulk Heterojunction Polymer Solar Cells. *Chem. Rev.* **2015**, *115*, 12666−12731.

(4) Thompson, B. C.; Frechet, J. M. Polymer-Fullerene Composite Solar Cells. *Angew. Chem., Int. Ed.* **2008**, *47*, 58−77.

(5) Green, M. A.; Emery, K.; Hishikawa, Y.; Warta, W.; Dunlop, E. D.; Levi, D. H.; Ho-Baillie, A. W. Y. Solar Cell Efficiency Tables (Version 49). *Prog. Photovoltaics* **2017**, *25*, 3−13.

(6) Hoppe, H.; Sariciftci, N. S. Morphology of Polymer/Fullerene Bulk Heterojunction Solar Cells. *J. Mater. Chem.* **2006**, *16*, 45−61.

(7) Dang, M. T.; Hirsch, L.; Wantz, G.; Wuest, J. D. Controlling the Morphology and Performance of Bulk Heterojunctions in Solar Cells. Lessons Learned from the Benchmark Poly(3-Hexylthiophene):[6,6]-Phenyl-C61-Butyric Acid Methyl Ester System. *Chem. Rev.* **2013**, *113*, 3734−3765.

(8) Chang, M.-Y.; Chen, Y.-F.; Tsai, Y.-S.; Chi, K.-M. Blending Platinum Nanoparticles into Poly(3-Hexylthiophene):[6,6]-Phenyl-C[Sub 61]-Butyric Acid Methyl Ester Enhances the Efficiency of Polymer Solar Cells. *J. Electrochem. Soc.* **2009**, *156*, B234−B237.

(9) Yu, H.; Ge, Y.; Shi, S. Improving Power Conversion Efficiency of Polymer Solar Cells by Doping Copper Phthalocyanine. Electrochim. *Electrochim. Acta* **2015**, *180*, 645−650.

(10) Haneline, M. R.; Tsunoda, M.; Gabbai, F. P. π-Complexation of Biphenyl, Naphthalene, and Triphenylene to Trimeric Perfluoro-Ortho-Phenylene Mercury. Formation of Extended Binary Stacks with Unusual Luminescent Properties. *J. Am. Chem. Soc.* **2002**, *124*, 3737−3742.

DOI: 10.1021/acs.chemmater.8b02152
Chem. Mater. 2018, 30, 5968−5977

(11) King, J. B.; Tsunoda, M.; Gabbai, F. P. Complexation of Aldehydes and Ketones by Trimeric Perfluoro-Ortho-Phenylene Mercury, a Tridentate Lewis Acid. *Organometallics* **2002**, *21*, 4201−4205.
(12) Omary, M. A.; Kassab, R. M.; Haneline, M. R.; Elbjeirami, O.; Gabbai, F. P. Enhancement of the Phosphorescence of Organic Luminophores Upon Interaction with a Mercury Trifunctional Lewis Acid. *Inorg. Chem.* **2003**, *42*, 2176−2178.
(13) Burress, C. N.; Bodine, M. I.; Elbjeirami, O.; Reibenspies, J. H.; Omary, M. A.; Gabbai, F. P. Enhancement of External Spin-Orbit Coupling Effects Caused by Metal-Metal Cooperativity. *Inorg. Chem.* **2007**, *46*, 1388−1395.
(14) Taylor, T. J.; Elbjeirami, O.; Burress, C. N.; Tsunoda, M.; Bodine, M. I.; Omary, M. A.; Gabbaï, F. P. Complexation of Tolane by Fluorinated Organomercurials—Structures and Luminescence Properties of an Unusual Class of Supramolecular π-Coordination Polymers. *J. Inorg. Organomet. Polym. Mater.* **2008**, *18*, 175−179.
(15) Burini, A.; Fackler, J. P.; Galassi, R.; Grant, T. A.; Omary, M. A.; Rawashdeh-Omary, M. A.; Pietroni, B. R.; Staples, R. J. Supramolecular Chain Assemblies Formed by Interaction of a π Molecular Acid Complex of Mercury with π-Base Trinuclear Gold Complexes. *J. Am. Chem. Soc.* **2000**, *122*, 11264−11265.
(16) Yu, G.; Gao, J.; Hummelen, J. C.; Wudl, F.; Heeger, A. J. Polymer Photovoltaic Cells - Enhanced Efficiencies Via a Network of Internal Donor-Acceptor Heterojunctions. *Science* **1995**, *270*, 1789−1791.
(17) Shaheen, S. E.; Brabec, C. J.; Sariciftci, N. S.; Padinger, F.; Fromherz, T.; Hummelen, J. C. 2.5% Efficient Organic Plastic Solar Cells. *Appl. Phys. Lett.* **2001**, *78*, 841−843.
(18) Zhang, F. L.; Johansson, M.; Andersson, M. R.; Hummelen, J. C.; Inganas, O. Polymer Photovoltaic Cells with Conducting Polymer Anodes. *Adv. Mater.* **2002**, *14*, 662−665.
(19) Liao, H.-C.; Ho, C.-C.; Chang, C.-Y.; Jao, M.-H.; Darling, S. B.; Su, W.-F. Additives for Morphology Control in High-Efficiency Organic Solar Cells. *Mater. Today* **2013**, *16*, 326−336.
(20) Liu, J.; Shi, Y.; Yang, Y. Solvation-Induced Morphology Effects on the Performance of Polymer-Based Photovoltaic Devices. *Adv. Funct. Mater.* **2001**, *11*, 420−424.
(21) Hoppe, H.; Niggemann, M.; Winder, C.; Kraut, J.; Hiesgen, R.; Hinsch, A.; Meissner, D.; Sariciftci, N. S. Nanoscale Morphology of Conjugated Polymer/Fullerene-Based Bulk- Heterojunction Solar Cells. *Adv. Funct. Mater.* **2004**, *14*, 1005−1011.
(22) Price, R. S. Excited State Properties of Organic and Organometallic Oligomers, Polymers and Materials and Their Solid-State Applications. Ph.D. Dissertation, University of Florida, Gainesville, FL, 2013. https://schanzelab.org/dissertations/.
(23) Collison, C. J.; Rothberg, L. J.; Treemaneekarn, V.; Li, Y. Conformational Effects on the Photophysics of Conjugated Polymers: A Two Species Model for MEH-PPV Spectroscopy and Dynamics. *Macromolecules* **2001**, *34*, 2346−2352.
(24) Taylor, T. J.; Burress, C. N.; Gabbaï, F. P. Lewis Acidic Behavior of Fluorinated Organomercurials. *Organometallics* **2007**, *26*, 5252−5263.
(25) Menon, A.; Galvin, M.; Walz, K. A.; Rothberg, L. Structural Basis for the Spectroscopy and Photophysics of Solution-Aggregated Conjugated Polymers. *Synth. Met.* **2004**, *141*, 197−202.
(26) Nguyen, T. Q.; Doan, V.; Schwartz, B. J. Conjugated Polymer Aggregates in Solution: Control of Interchain Interactions. *J. Chem. Phys.* **1999**, *110*, 4068−4078.
(27) Panzer, F.; Bassler, H.; Kohler, A. Temperature Induced Order-Disorder Transition in Solutions of Conjugated Polymers Probed by Optical Spectroscopy. *J. Phys. Chem. Lett.* **2017**, *8*, 114−125.
(28) Sherwood, G. A.; Cheng, R.; Smith, T. M.; Werner, J. H.; Shreve, A. P.; Peteanu, L. A.; Wildeman, J. Aggregation Effects on the Emission Spectra and Dynamics of Model Oligomers of MEH-PPV. *J. Phys. Chem. C* **2009**, *113*, 18851−18862.
(29) Careful inspection of the negative signal between 575 and 600 nm in Figure 2B reveals that, at longer delay times, the peak negative signal blue-shifts so that it corresponds to the peak ground state absorption of the aggregate. This implies that the polaron is localized in the aggregated domain of the polymer.
(30) Candeias, L. P.; Grozema, F. C.; Padmanaban, G.; Ramakrishnan, S.; Siebbeles, L. D. A.; Warman, J. M. Positive Charge Carriers on Isolated Chains of MEH-PPV with Broken Conjugation: Optical Absorption and Mobility. *J. Phys. Chem. B* **2003**, *107*, 1554−1558.
(31) Alem, S.; de Bettignies, R.; Nunzi, J.-M.; Cariou, M. Efficient Polymer-Based Interpenetrated Network Photovoltaic Cells. *Appl. Phys. Lett.* **2004**, *84*, 2178−2180.
(32) Yang, C. Y.; Hide, F.; Diaz-Garcia, M. A.; Heeger, A. J.; Cao, Y. Microstructure of Thin Films of Photoluminescent Semiconducting Polymers. *Polymer* **1998**, *39*, 2299−2304.
(33) Osaka, I.; Takimiya, K. Backbone Orientation in Semiconducting Polymers. *Polymer* **2015**, *59*, A1−A15.
(34) Kawashima, K.; Tamai, Y.; Ohkita, H.; Osaka, I.; Takimiya, K. High-Efficiency Polymer Solar Cells with Small Photon Energy Loss. *Nat. Commun.* **2015**, *6*, 10085.
(35) Jeng, U.; Hsu, C. H.; Sheu, H. S.; Lee, H. Y.; Inigo, A. R.; Chiu, H. C.; Fann, W. S.; Chen, S. H.; Su, A. C.; Lin, T. L.; Peng, K. Y.; Chen, S. A. Morphology and Charge Transport in Poly(2-Methoxy-5-(2'-Ethylhexyloxy)-1,4-Phenylenevinylene) Films. *Macromolecules* **2005**, *38*, 6566−6574.
(36) Hoofman, R. J. O. M.; de Haas, M. P.; Siebbeles, L. D. A.; Warman, J. M. Highly Mobile Electrons and Holes on Isolated Chains of the Semiconducting Polymer Poly(Phenylenevinylene). *Nature* **1998**, *392*, 54−56.
(37) Cornil, J.; Beljonne, D.; Calbert, J. P.; Bredas, J. L. Interchain Interactions in Organic π-Conjugated Materials: Impact on Electronic Structure, Optical Response, and Charge Transport. *Adv. Mater.* **2001**, *13*, 1053−1067.
(38) Tessler, N.; Preezant, Y.; Rappaport, N.; Roichman, Y. Charge Transport in Disordered Organic Materials and Its Relevance to Thin-Film Devices: A Tutorial Review. *Adv. Mater.* **2009**, *21*, 2741−2761.
(39) Bredas, J. L.; Norton, J. E.; Cornil, J.; Coropceanu, V. Molecular Understanding of Organic Solar Cells: The Challenges. *Acc. Chem. Res.* **2009**, *42*, 1691−1699.
(40) Wang, C.; Dong, H.; Hu, W.; Liu, Y.; Zhu, D. Semiconducting π-Conjugated Systems in Field-Effect Transistors: A Material Odyssey of Organic Electronics. *Chem. Rev.* **2012**, *112*, 2208−2267.
(41) Chistyakov, A. L.; Stankevich, I. V.; Gambaryan, N. P.; Struchkov, Y. T.; Yanovsky, A. I.; Tikhonova, I. A.; Shur, V. B. Crown Compounds for Anions. A New Approach to the Description of Chemical Bonds in the Complexes of Halide Anions with Polymercury-Containing Macrocycles. *J. Organomet. Chem.* **1997**, *536*−*537*, 413−424.

DOI: 10.1021/acs.chemmater.8b02152
Chem. Mater. 2018, 30, 5968−5977